PHYSICAL REVIEW B **82**, 201101(R) (2010)

Interface band profiles of Mott-insulator/Nb:$SrTiO_3$ heterojunctions as investigated by optical spectroscopy

Masao Nakamura,[1,*] Akihito Sawa,[2] Jun Fujioka,[3] Masashi Kawasaki,[1,4] and Yoshinori Tokura[1,3,5]

[1]*Cross-Correlated Materials Research Group (CMRG) and Correlated Electron Research Group (CERG), ASI, RIKEN, Wako 351-0198, Japan*

[2]*National Institute of Advanced Industrial Science and Technology (AIST), Tsukuba 305-8562, Japan*

[3]*Multiferroic Project, Exploratory Research for Advanced Technology (ERATO), Japan Science and Technology Agency (JST), Kawaguchi 332-0012, Japan*

[4]*WPI-Advanced Institute for Materials Research (AIMR), Tohoku University, Sendai 980-8577, Japan*

[5]*Department of Applied Physics, University of Tokyo, Tokyo 113-8656, Japan*

(Received 21 October 2010; published 5 November 2010)

Heterointerfaces of correlated electron oxides provide a good laboratory to explore novel electronic states induced by the coupling among spin, charge, and orbital degrees of freedom. For the detail understanding of the complex interface states, it is indispensable to elucidate the interface band profiles of correlated electron materials. Here we report the band profiles of Mott-insulator/Nb:$SrTiO_3$ heterojunctions revealed by optical-spectroscopic and transport measurements. Photocurrent action spectra indicate the existence of the band bending and band discontinuity similar to the rigid-band interface and we construct a band lineup of Mott insulators based on the rigid-band picture. We also estimate the width of the depletion layer in a Mott insulator by investigating thickness dependence of photocurrent amplitude.

DOI: 10.1103/PhysRevB.82.201101 PACS number(s): 73.20.−r, 73.40.Lq, 79.60.Jv

There have been growing interests on heterointerfaces of complex oxides triggered by marked advances in the technique of the thin-film growth. The most distinctive feature of the complex oxides from conventional materials such as semiconductors (doped-band-insulators) is a wide variety of electronic phases induced by the inherent strong electron correlation. After pioneering works by Ohtomo *et al.*[1] and Okamoto and Millis[2] a lot of experimental observations and theoretical predictions have revealed the unprecedented interface electronic states in oxide heterojunctions. The oxide heterointerface is also attractive from the view point of application to novel storage or photovoltaic devices. For engineering the interface electronic states as well as designing possible devices, the basic knowledge on band profiles of the correlated electron interface is indispensable.

To establish the band lineup, which maps out the relative positions of the energy bands for constituent materials, is prerequisite for predicting the interface band profile. Once the band lineup is known, one can model the band profile and charge distribution at the interface of materials with a given doping level, assuming an ideal junction of rigid-band materials.[3] This is also the case for interfaces of correlated electron materials, although the electron correlation may modify the interface band structure.[4,5] Therefore, to clarify the origin of the complex feature of the correlated interface, it is extremely useful to analyze the interface band profile on the basis of rigid-band model. Then, one may be able to explore the differences, i.e., the effects of electron correlation, from the interface of conventional semiconductors. Here we report interface band profiles of Mott-insulator/doped-band-insulator heterojunctions and a band lineup of Mott insulators revealed by photocurrent action and absorption spectroscopies as well as transport measurements. It was found out that the interface band structures of the Mott insulators are well approximated by the rigid-band picture in the light doping regime. Although the one-electron rigid-band picture has been already used as an assumption to model the interface band structure of complex oxides relying on only transport data in previous reports, we derived this conclusion without any assumptions but by combining optical and transport measurements in this study. The effect of strong electron correlation shows up as a short diffusion length of minority carriers.

The compounds investigated here are prototypical Mott insulators—La_2CuO_4 (LCO), Sm_2CuO_4 (SCO), $LaMnO_3$ (LMO), and $SrMnO_3$ (SMO), which are well known as parent compounds of high-T_c-superconducting cuprates or colossal-magnetoresistive manganites. All of them are typical Mott insulators with antiferromagnetic orders in their ground states. LCO and LMO are *p*-type Mott insulators, where a slight amount of inherent defects or an intentional band filling control can generate majority hole carriers, whereas SCO and SMO are *n*-type Mott insulators. These Mott insulators were grown on Nb 0.02 at. % doped $SrTiO_3$ (Nb:STO) which is an electron-doped band insulator to construct *p-N* or *n-N* Mott-insulator/doped-band-insulator heterojunctions. Hereafter we abbreviate Nb:STO layer as *N* layer and Mott-insulators layer as *p* or *n* layer. Such heterojunctions have been known to show a highly rectifying behavior.[6–12] As shown in Fig. 1, all the Mott-insulator/Nb:STO heterojunctions fabricated in this study similarly show a clear character of diode with high rectification ratios. They also show the linearity between the inverse square of the capacitance (C^{-2}) and the applied voltage (V), in accord with the results of former studies. In the scheme of the rigid-band *p-N* junction, the capacitance is related to the applied voltage by

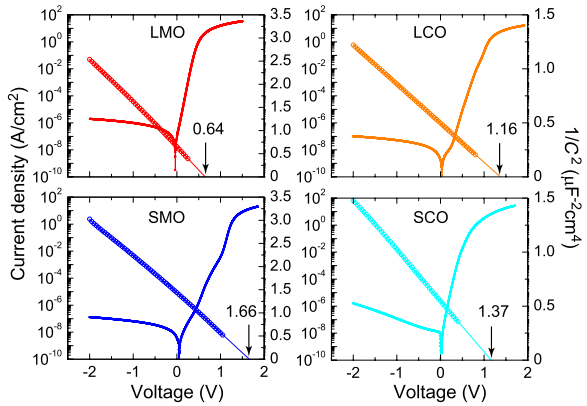

FIG. 1. (Color online) Current density (J)-voltage (V) (solid line for left axis) and capacitance (C)-voltage (V) characteristics of Mott-insulator/Nb:$SrTiO_3$ (Nb:STO) heterojunctions measured at ambient temperature. Among the four compounds, LMO and LCO are p-type Mott-insulators and the others, SMO and SCO are n-type ones. The arrows indicate the voltage-axis intercept points of the linear extrapolation of C^{-2}-V plot. Their values shown in each panel in a unit of electron volts represent the built-in potentials of the junctions.

$$\frac{1}{C^2} = \frac{2}{q}\left(\frac{1}{\varepsilon_p n_p} + \frac{1}{\varepsilon_N n_N}\right)(V_{bi} - V), \tag{1}$$

where V_{bi} is the built-in voltage, $n_p(n_N)$ and $\varepsilon_p(\varepsilon_N)$ are the carrier density and the dielectric constant in $p(N)$ layer, respectively.[3] We can directly derive the built-in potential (qV_{bi}) from the intercept point on the voltage axis which corresponds to the energy difference in the Fermi levels of contacting materials. Although the formula is rather complex in n-N junctions, the voltage intercept point is approximated to be the built-in potential if $\varepsilon_n n_n \gtrsim \varepsilon_N n_N$.[10] The deduced built-in potential values are 0.64 eV for LMO, 1.37 eV for LCO, 1.66 eV for SMO, and 1.16 eV for SCO.

The change in the capacitance mainly comes from the change in depletion layer thickness in Nb:STO because n_N is about 1×10^{18} cm^{-3} and much smaller than the activated carrier density of usual Mott insulators at room temperature over 1×10^{19} cm^{-3}.[13] Thus, the linear gradient of the C^{-2}-V plot reveals that the product of ε_N and n_N is constant along depth direction in Nb:STO. (Note that there are differences in the slope of C^{-2}-V plot from sample to sample by a factor of about 3. This is because the dopant activation ratio in such a lightly doped STO is critically affected by the crystal quality and the actual carrier concentration widely varies depending on an adopted substrate sample).[14] This analysis, however, gives little information on the interface band profiles of Mott insulators. We employed photocurrent action spectroscopy known as a good probe of band structures near buried interfaces to unveil interface electronic structures of the Mott insulators.[15]

Photocurrent action spectra were taken by irradiating a monochromatic light from a xenon or halogen lamp chopped at 270 Hz and measuring induced current synchronized with the chopping frequency with a lockin amplifier. For the measurements, the junctions were patterned into a mesastructure

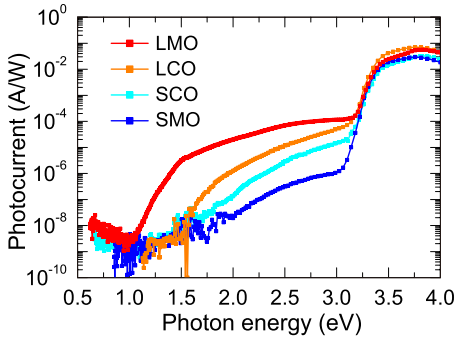

FIG. 2. (Color online) Photocurrent action spectra normalized by monochromatic light intensity for Mott-insulator/Nb:$SrTiO_3$ heterojunctions.

with an area of 200×200 μm^2 on which the incident light was focused. (Details of the device structure and fabrication process were given in Ref. 10.) We also measured the absorption spectra of the Mott insulators to deduce their optical gaps. The measurement was performed on the films grown on nondoped STO substrates.

In Fig. 2 are displayed photocurrent action spectra for all the junctions. The steep increase above 3.2 eV is due to the onset of interband excitation in Nb:STO. The photoexcited electrons and holes are spatially separated by the electric field in the depletion layer of Nb:STO and contribute to the photocurrent. Below the absorption edge of Nb:STO, the spectra show differences in their amplitude as well as threshold energy. One prominent feature is that the junctions of p-type Mott insulators exhibit larger photocurrent and low threshold energy compared with those of n-type ones.

To clarify the origin of these differences, we compare in Fig. 3(a) the linear absorption spectra and threshold regions of the photocurrent action spectra. In the p-N junctions, the photocurrent starts to appear at the photon energy almost coincident with the optical gap. This result indicates that the photoexcited electrons and holes in the Mott insulator near the interface are spatially separated through diffusion or drift processes of minority carriers (electrons) across the interface (length scale of these processes is about 6 nm as discussed later). Therefore, one can deduce a band profile of the p-N junction assuming rigid band as depicted in the left schematic of Fig. 3(b).

On the contrary, the photocurrent in n-N junctions appears from a higher energy than the optical gap by 1.55 eV for SMO and 0.66 eV for SCO. This means that the photocurrent is not generated even though photons are absorbed in this energy region. We can explain this feature as follows on the basis of the band profile of the rigid-band model depicted in the right schematic of Fig. 3(b). In n-N junctions, the difference in the conduction-band position causes a potential barrier for photoexcited electrons in the n layer to flow into the N layer. Therefore, the photocurrent appears from the photon energy of the optical gap plus the conduction-band offset.[16] The energy of conduction-band offset (ΔE_c) is related to the built-in potential as $\Delta E_c = qV_{bi} - \delta_n + \delta_N$, where δ_n and δ_N refer to the position of the Fermi energy relative to the conduction-band minimum in n and N layer, respectively. Since δ_N of the lightly electron-doped STO is negligibly

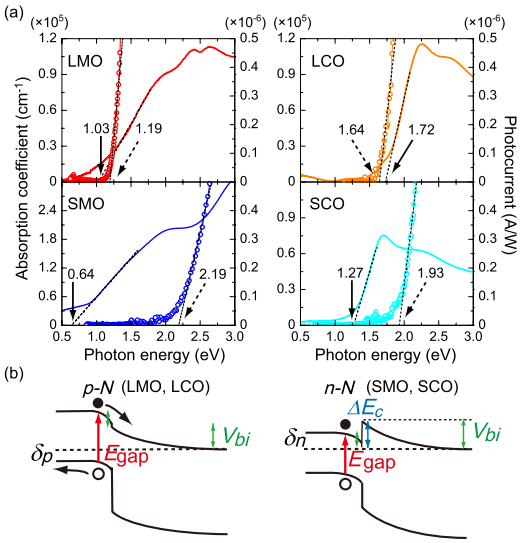

FIG. 3. (Color online) (a) Absorption spectra (solid line for left axis) of the Mott insulator thin films and the threshold regions of the photocurrent action spectra (open circles for right axis) of the Mott-insulator/Nb:$SrTiO_3$ heterojunctions (right axis). The optical gap (E_{gap}) was estimated from linear extrapolation of the absorption edge as shown by solid arrows and broken lines, respectively. The threshold energies of the photocurrent action spectra (E_{th}) are indicated by dashed arrows. (b) Schematic band profiles deduced for the *p-N* (left) and *n-N* (right) junctions composed of Mott insulators and Nb:STO. Photocurrent can appear when the irradiated photon energy exceeds the optical gap ($E_{th}=E_{gap}$) as shown for *p-N* junctions. When there are spike and notch in the conduction-band profile at the interface, photon energy has to exceed $E_{gap}+\Delta E_c$, where ΔE_c is the conduction-band offset.

small (40 meV),[17] δ_n is estimated to be 0.11 eV in SMO and 0.50 eV in SCO.

From these results based on the rigid-band picture, we deduce the band lineup of the Mott insulators as depicted in Fig. 4. The Fermi energy of *p*-type LCO is lower than those of *n*-type SCO while that of *p*-type LMO and *n*-type SMO are in the reversed relation. This is consistent with the result of x-ray photoemission spectroscopy (XPS) performed for bulk compounds.[18,20,22,23] The contrastive relation is due to the difference in the factor that determines the carrier type of the Mott insulator. The filling of e_g band is the origin of the opposite carrier type between LMO (d^4) and SMO (d^3) while the difference in the crystal structure, the so-called *T* structure in LCO and *T′* structure in SCO, defines their carrier types.[24] The energy differences in the Fermi level between *n*-type and *p*-type Mott insulators (ΔE_{np}) deduced from the present experiments is −1.0 eV in the manganites and 0.2 eV in the cuprates. According to the results of XPS, ΔE_{np} is estimated −0.7∼−0.9 eV for the manganite[22,23] and 0.3 eV for the cuprates.[18,20] The close agreement between the present data and the XPS data for bulk crystals signifies that the rigid-bandlike band profiles depicted in Fig. 3(b) provide a good approximation to represent the interface band structure of Mott-insulator/Nb:STO junctions.

Hereafter we estimate the width of depletion layer in a Mott insulator from the thickness dependence of photocurrent amplitude. LMO/Nb:STO films with different thicknesses ranging from 2 to 40 nm were prepared and their photocurrent action spectra were measured in the same way as described above. The obtained external quantum efficiency of photocurrent generation at photon energies of 2.5 and 3.5 eV are shown in Fig. 5. The quantum efficiency at 2.5 eV has a maximum at around 6 nm while that obtained at 3.5 eV shows a monotonic decrease as LMO thickness increases because the photoexcitation of Nb:STO band gap is the dominant origin of the photocurrent at this photon energy and the photon absorption in LMO layer reduces the incident light reaches to Nb:STO layer. We consider the thickness dependence at 2.5 eV on the assumption that the efficiency of the photocurrent generation is proportional to the number of photons absorbed in the depletion layer plus the neighboring layer within the width of diffusion length of minority

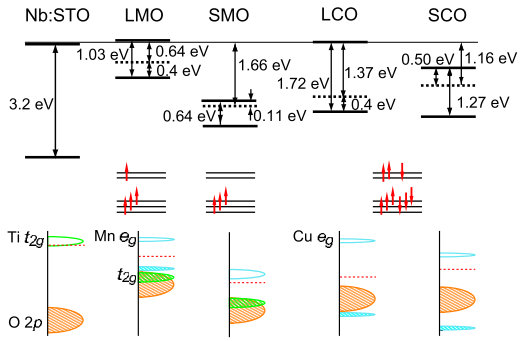

FIG. 4. (Color online) Band lineup of the Mott insulators relative to the energy level of Nb:$SrTiO_3$ deduced from the built-in potentials, optical gap, and the threshold energy of the photocurrent action spectra. Lines in top panel are conduction- and valence-band edges in the frame work of rigid-band picture. The broken lines are Fermi level. Since the present method is unable to estimate the Fermi energy of *p*-type Mott insulators relative to the valence-band maximum (δ_p), we use the values reported for bulk compounds [about 0.4 eV both for LMO and LCO (Refs. 18 and 19)]. The bottom panel is the schematic band structure for *d* and *p* states of transition metals and oxygen, respectively, for which filled states are hatched and Fermi level is shown by broken line. Photoemission data (Refs. 18–21) are referred for the orbital identity of the conduction (or unoccupied) and valence (or occupied) bands of the Mott insulators. Spin configurations are also shown for 3*d* orbitals in Mn and Cu.

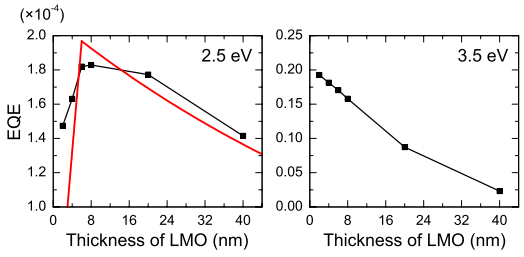

FIG. 5. (Color online) External quantum efficiency of photocurrent generation for LMO/Nb:STO junctions as a function of the thickness of LMO. Measurements were performed at the photon energies of 2.5 and 3.5 eV. The solid line in the left panel is a plot of Eq. (2), calculated with W_p+L_p fixed to 6 nm and $\alpha(\omega)$ shown in Fig. 3. J_0 is a fitting parameter.

carrier in LMO, which is the so-called effective thickness. Then, the quantum efficiency is given as a function of the film thickness d like

$$J = J_0(1 - e^{-\alpha d})(d < W_p + L_p),$$

$$J = J_0(e^{-\alpha(d-W_p-L_p)} - e^{-\alpha d})(d \geq W_p + L_p), \quad (2)$$

where α is the absorption coefficient of LMO, W_p the width of depletion layer in LMO, L_p the diffusion length of electron in LMO, and J_0 a constant. We plot the function with a solid line in Fig. 5 by using the value W_p+L_p fixed to 6 nm and α shown in Fig. 3(a). The function well reproduces the decay of the quantum efficiency with increasing the thickness above 6 nm. Therefore, it is plausible to consider that the width of depletion layer in LMO is shorter than 6 nm and minority-carrier diffusion length is also quite short compared with that in conventional semiconductors that reaches several hundred micrometers. The reason for the short depletion width is the large residual carrier density in the Mott insulators while the short diffusion length is caused by the strong electron correlation which enhances the effective carrier mass and lowers the electron mobility.

The present results elucidate the validity of the interface band profiles of Mott insulators within the framework of the rigid-band picture for this doping regime. The charge redistribution derived by the Fermi-level difference affects a tiny perturbation on the band alignment of Mott insulators. This result is quite surprising and somewhat puzzling because it is commonly believed that the rigid-band picture always fails to explain the collective responses of Mott insulators. The present puzzling but usefully simple aspect of the correlated electron heterointerface will invoke vigorous theoretical efforts hereafter. Of course, an intentional charge modulation by applying external fields will make obvious the electron correlation effect in Mott insulators as an interface electronic reconstruction,[6,8,10] where we expect a large field response and nontrivial electronic states. Even in that case, the genuine band profiles as revealed here will determine whether the applied field can deplete or accumulate charge carriers at interface.

In summary, we have investigated interface band profiles of Mott-insulator/Nb:$SrTiO_3$ p-N or n-N heterojunctions by using photocurrent action and absorption spectroscopies combined with transport measurements. Photocurrent action spectra have revealed the existence of the depletion layer in p-N junctions and the conduction-band offset in the n-N junctions, which are well consistent with the band profile based on the hypothesis that the interface of Mott insulator keeps a bulklike band structure. The presently established band lineup of Mott insulators will give a basic guideline to design or predict functionalities in the heterostructures of correlated electron materials.

We thank H. Sato and H. Akoh for the help of device fabrication, T. Hasegawa for the use of spectrometer, and Y. Taguchi and H. Wadati for fruitful discussions. This work was partly supported by the MEXT of Japan through its Grant-in-Aid for Young Scientists (B) under Grant No. 21760032, New Energy and Industrial Technology Development Organization (NEDO), and Japan Society for the Promotion of Science (JSPS) through its "Funding Program for World-Leading Innovative R&D on Science and Technology (FIRST Program)."

*masao.nakamura@riken.jp

[1] A. Ohtomo, D. A. Muller, J. L. Grazul, and H. Y. Hwang, Nature (London) **419**, 378 (2002).
[2] S. Okamoto and A. J. Millis, Nature (London) **428**, 630 (2004).
[3] S. M. Sze, *Physics of Semiconductor Devices*, 2nd ed. (Wiley, New York, 1981).
[4] W.-C. Lee and A. H. MacDonald, Phys. Rev. B **74**, 075106 (2006).
[5] S. Yunoki, A. Moreo, E. Dagotto, S. Okamoto, S. S. Kancharla, and A. Fujimori, Phys. Rev. B **76**, 064532 (2007).
[6] H. Tanaka, J. Zhang, and T. Kawai, Phys. Rev. Lett. **88**, 027204 (2001).
[7] F. X. Hu, J. Gao, J. R. Sun, and B. G. Shen, Appl. Phys. Lett. **83**, 1869 (2003).
[8] Y. Muraoka, T. Muramatsu, J. Yamaura, and Z. Hiroi, Appl. Phys. Lett. **85**, 2950 (2004).
[9] A. Sawa, T. Fujii, M. Kawasaki, and Y. Tokura, Appl. Phys. Lett. **86**, 112508 (2005).
[10] M. Nakamura, A. Sawa, H. Sato, H. Akoh, M. Kawasaki, and Y. Tokura, Phys. Rev. B **75**, 155103 (2007).
[11] J. Fang, Y. Cui, Y. Zhang, and M. Qiu, Physica C **458**, 51 (2007).
[12] W. M. Lü, J. R. Sun, Y. Z. Chen, and B. G. Shen, Appl. Phys. Lett. **94**, 152514 (2009).
[13] S. Ono, S. Komiya, and Y. Ando, Phys. Rev. B **75**, 024515 (2007).
[14] T. Fujii, M. Kawasaki, A. Sawa, Y. Kawazoe, H. Akoh, and Y. Tokura, Phys. Rev. B **75**, 165101 (2007).
[15] Y. Hikita, Y. Kozuka, T. Susaki, H. Takagi, and H. Y. Hwang, Appl. Phys. Lett. **90**, 143507 (2007).
[16] S. R. Forrest and O. K. Kim, J. Appl. Phys. **52**, 5838 (1981).
[17] M. Takizawa, K. Maekawa, H. Wadati, T. Yoshida, A. Fujimori, H. Kumigashira, and M. Oshima, Phys. Rev. B **79**, 113103 (2009).
[18] H. Namatame *et al.*, Phys. Rev. B **41**, 7205 (1990).
[19] K. Horiba, A. Chikamatsu, H. Kumigashira, M. Oshima, N. Nakagawa, M. Lippmaa, K. Ono, M. Kawasaki, and H. Koinuma, Phys. Rev. B **71**, 155420 (2005).
[20] J. W. Allen *et al.*, Phys. Rev. Lett. **64**, 595 (1990).
[21] T. Saitoh, A. E. Bocquet, T. Mizokawa, H. Namatame, A. Fujimori, M. Abbate, Y. Takeda, and M. Takano, Phys. Rev. B **51**, 13942 (1995).
[22] J.-H. Park, C. T. Chen, S.-W. Cheong, W. Bao, G. Meigs, V. Chakarian, and Y. U. Idzerda, Phys. Rev. Lett. **76**, 4215 (1996).
[23] J. Matsuno, A. Fujimori, Y. Takeda, and M. Takano, Europhys. Lett. **59**, 252 (2002).
[24] Y. Tokura and T. Arima, Jpn. J. Appl. Phys., Part 1 **29**, 2388 (1990).